Urban Climate xxx (xxxx) xxx–xxx

Contents lists available at ScienceDirect

Urban Climate

journal homepage: www.elsevier.com/locate/uclim

A modeling study of the sensitivity of urban heat islands to precipitation at climate scales

Yaofeng Gu, Dan Li*

Department of Earth and Environment, Boston University, Boston, MA 02215, United States

ARTICLE INFO

Keywords:
Urban heat island
Precipitation
Urban canopy model
CONUS

ABSTRACT

The impacts of urban surface characteristics on urban heat islands have been extensively studied. However, the influence of local climate on the urban heat island intensity remains elusive. This study aims to quantify the influence of precipitation on the urban heat island intensity over the Continental United States (CONUS) at climate scales. Results from numerical experiments show that across the CONUS, the urban heat island intensities are positively correlated with the precipitation amounts in summer but not in winter. The sensitivity of urban heat island intensity to precipitation varies spatially and seasonally. In summer, the urban heat island intensity in mid-south CONUS is particularly sensitive to changes in precipitation and the sensitivity shows a generally negative correlation with the precipitation amount. The sensitivity is found to largely come from the rural temperature rather than the urban temperature, and is mostly controlled by the partition of available energy to sensible and latent heat fluxes. In winter the albedo effect is also important. This study highlights the climatic conditions as important controls on the urban heat island intensity, and thus climate change has significant implications for the urban thermal environment even if urban surface characteristics remain the same.

1. Introduction

The urban heat island (UHI) effect refers to a microclimatic phenomenon that cities are typically hotter than the surrounding rural areas (Oke, 1982; Arnfield, 2003; Grimmond, 2007; Mills, 2008). It has important implications for energy consumption (Akbari et al., 2001), human health (Anderson and Bell, 2009), air pollution (Sarrat et al., 2006), and biogeochemical cycles (Grimm et al., 2008). Given the fact more than half of the global population lives in cities now and the continued urbanization (United Nations, 2014), it becomes important to fully understand the causes of, and contributors to, UHIs, which will pave the way for developing strategies for mitigating heat in cities (Rizwan et al., 2008; Rosenzweig et al., 2010; Stone, 2012).

Studies on the UHI effect can be broadly separated into three categories: theoretical, experimental, and numerical studies. Theoretical studies often focus on the scaling of urban heat island intensity (UHII) (Fernando et al., 2010; Hidalgo et al., 2010; Fan et al., 2016; Theeuwes et al., 2017), which is often defined as the difference between urban and rural near-surface air (or surface) temperatures, with respect to city size (Oke, 1973), canyon geometry (Oke, 1981), wind speed (Li et al., 2016), urban-rural contrasts of water availability (Li and Bou-Zeid, 2013), and related parameters. Experimental studies often focus on quantifying the UHII using in situ and/or remotely sensed observational data and exploring their correlations with urban-rural contrasts of various biogeophysical factors (Schatz and Kucharik, 2014; Zhou et al., 2016) and hydroclimatic factors (Hoffmann et al., 2012; Wiesner et al., 2014). Over the last two decades, numerical studies have become popular and many urban models have been proposed to simulate

* Corresponding author.
E-mail address: lidan@bu.edu (D. Li).

https://doi.org/10.1016/j.uclim.2017.12.001
Received 12 April 2017; Received in revised form 7 October 2017; Accepted 8 December 2017

the urban thermal environment (Grimmond et al., 2010; Grimmond et al., 2011; Best and Grimmond, 2015). These models allow investigations of the sensitivity of UHII to a wide range of factors such as urban morphologies, surface materials, vegetation coverage and types, and anthropogenic activities (Loridan et al., 2010; Ryu et al., 2011; Wang et al., 2011).

Although it is well acknowledged that the UHII varies across different climatic conditions (Arnfield, 2003), a systematic investigation of how different climatic factors affect the UHII is lacking. Nonetheless, understanding the influence of climatic factors, in addition to the influence of surface characteristics, is important for capturing and forecasting the UHII under climate change. A recent study by Zhao et al. (2014) demonstrated strong contributions of background climate to urban heat islands by showing that the annual mean daytime UHII across the North America is strongly and positively correlated with the annual mean precipitation amount. However, their study did not compare directly the influence of precipitation on the UHII to the influences of other climatic variables. In addition, they did not examine the seasonality of the sensitivity of UHII to precipitation. These remaining questions motivate our study.

Using offline land simulations with the Geophysical Fluid Dynamics Laboratory (GFDL) land model coupled with a newly developed and validated urban canopy model (Li et al., 2016a), this study analyzes the influence of atmospheric forcing, especially precipitation, on simulated urban heat islands over the Continental United States (CONUS). The specific questions we aim to answer in this paper include: 1) how important is the influence of atmospheric forcing, particularly precipitation, in controlling the simulated UHII in different seasons? 2) Does the sensitivity of UHII to precipitation differ between regions and seasons?

The rest of the paper is organized as follows: Section 2 describes the model and methodology; Section 3 presents the main results; and Section 4 summarizes the findings and discusses the implications.

2. Model and methodology

The model used in this study is the land component (called LM3) of GFDL global climate and earth system models, coupled with a newly developed and validated urban canopy model (UCM). Details about the LM3 (Shevliakova et al., 2009; Milly et al., 2014) and the LM3-UCM (Li et al., 2016a), including model validation, have been described elsewhere. Here only the key features are introduced. LM3 represents each grid-cell's surface heterogeneity as a collection of tiles (Shevliakova et al., 2009; Milly et al., 2014). Each tile has its own energy and water balances throughout the vegetation-soil column and its own exchange coefficients with the atmosphere. The fluxes of each tile are aggregated at the bottom atmospheric layer so that the atmosphere only receives the area-averaged fluxes. The principle land cover types in LM3 include natural vegetation, grassland, pasture, secondary vegetation, and urban. The LM3-UCM is built on the urban canyon concept and includes two major components: roof and canyon (Li et al., 2016a). It solves the surface energy balance for different urban facets, including roof, wall, impervious ground, and pervious ground. It considers radiation processes in the urban canyon including radiative trapping, shadow effects, and multiple reflections between walls and ground surfaces. It parameterizes turbulent exchanges between the atmosphere, the canopy air, walls and ground surfaces through a resistance approach. It also incorporates hydrological and biological processes associated with vegetation within the urban canyon.

In this study, the LM3 is driven by atmospheric forcing from large-scale climate model outputs or gridded data sets that are primarily based on observations and reanalysis fields to simulate the UHII. The forcing variables for all experiments include downward shortwave radiation, downward longwave radiation, air temperature, specific humidity, pressure, wind speed, and precipitation. In the first experiment (see Table 1), outputs at the bottom level of the atmospheric component from coupled land-atmosphere-ocean earth system model simulations for the Coupled Model Intercomparison Project Phase 5 (CMIP5) are used. Specifically, ESM2Mb model outputs (Dunne et al., 2012; Dunne et al., 2013; Malyshev et al., 2015), with a spatial resolution of 2 by 2.5° and a temporal resolution of three hours, are used to conduct long-term simulations (from 1700 to 2100) over North America (20°N–55°N, 130°W–60°W). This is identical to the simulation presented in Li et al. (2016b). In the second experiment (Exp. 2), the LM3 is also driven by a 50-yr (1949–2000), 3-hourly, 1-degree data set developed by Sheffield et al. (2006) (hereafter called Princeton forcing), which is based on a combination of observational and reanalysis data. We apply the first 30-yr forcing to the period of 1700–1948 in order to spin-up the model. Given the difference in the resolution of the two forcing data sets, both are then interpolated to a grid of resolution of 50 km for a consistent comparison. In all the experiments, we focus on the period from 1981 to 2000.

To examine the role of precipitation in controlling the UHII across the North America, we also design a third experiment (Exp. 3), in which the model is driven by atmospheric forcing used for Exp. 1 except that the precipitation data are replaced by those from Exp. 2. While we acknowledge that mixing the two forcing data sets may introduce inconsistency between precipitation and other forcing variables, this issue should be alleviated at the temporal scale that we are interested in (i.e., the long-term scale). Given that the precipitation from Exp. 2 is corrected by observations, our third experiment is essentially similar to many previous studies, including

Table 1
The list of numerical experiments.

Experiments	Key features
1	ESM2Mb forcing;
2	Princeton forcing;
3	ESM2Mb forcing except that precipitation is from Princeton forcing;

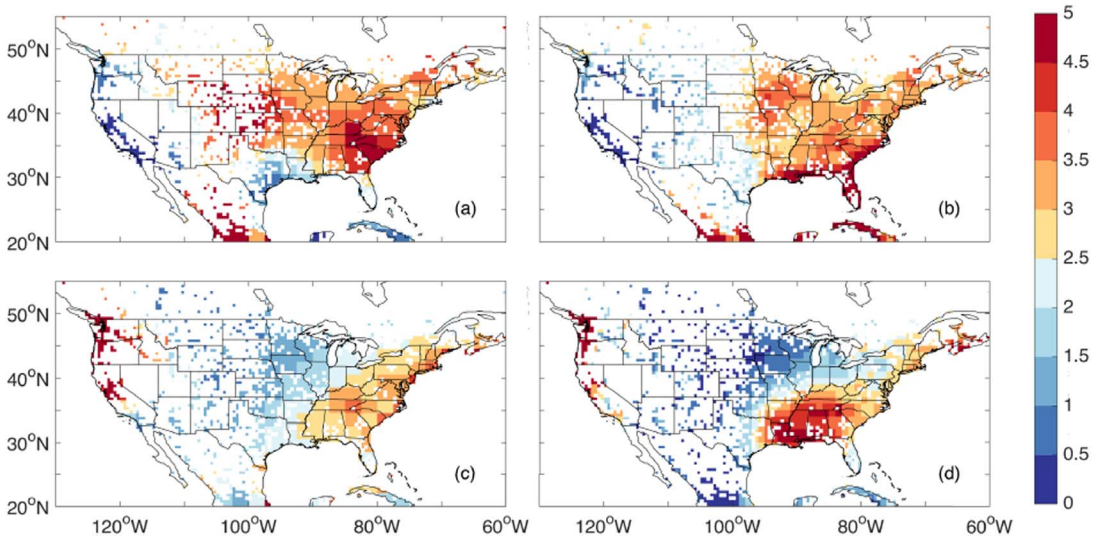

Fig. 1. The spatial patterns of precipitation (unit: mm/day) in ESM2Mb (a, c) and Princeton forcing (b, d) in summer (a, b) and winter (c, d).

those producing the Princeton forcing (Sheffield et al., 2006) and the MERRA-Land data set (Reichle et al., 2011), which use model outputs or reanalysis fields as the basis and corrects some fields (in this case precipitation) with observations. Fig. 1 compares the spatial patterns of precipitation in these two forcing data sets in summer and winter. It is clear that the spatial patterns are in fairly good agreement, which suggests that Exp. 3 mainly alters the magnitude of precipitation but not the spatial structure. Given that the Princeton forcing is based on reanalysis fields and observational data, the good agreement also signifies the good performance of ESM2Mb in capturing the spatial patterns of precipitation in both summer and winter.

To quantify the sensitivity of UHII to precipitation, we calculate the partial derivative of UHII with respect to precipitation following

$$\frac{\partial UHII}{\partial P} = \frac{UHII\,(Exp.3) - UHII\,(Exp.1)}{P\,(Exp.3) - P\,(Exp.1)} \tag{1}$$

This is because the only difference between Exp. 3 and Exp. 1 is the precipitation forcing. We further denote $\Delta P = P(Exp.\ 3) - P(Exp.\ 1)$ and $\Delta UHII = UHII(Exp.\ 3) - UHII(Exp.\ 1)$, hence $\Delta UHII = (\partial UHII/\partial P)\ \Delta P$.

In addition, to quantify the importance of precipitation among all forcing variables, we define the index

$$R_1 = \frac{UHII\,(Exp.3) - UHII\,(Exp.1)}{UHII\,(Exp.2) - UHII\,(Exp.1)}. \tag{2}$$

This index represents the influence of precipitation on the UHII normalized by the influence of all forcing variables because Exp. 2 changes all the forcing variables while Exp. 3 only changes the precipitation when compared to Exp. 1. As such, a larger R_1 indicates that precipitation is more important in controlling the UHII.

In our study, the UHII is defined as the canopy air temperature difference between urban and rural land within the same grid cell. Canopy air temperature is not specifically tied to urban canopies but rather a term used to distinguish from reference temperature that is often reported at 2 m above the displacement height (see Malyshev et al. (2015) for more detailed discussions). The rural temperature is defined as the average of all non-urban, vegetation (i.e., natural and secondary vegetation, grassland, and pasture) temperatures. We also examined the results using only the temperature of natural vegetation as the rural reference and found that although the resulting UHII differs, the spatial pattern of UHII is not altered, which is similar to the finding of previous studies (Zhou et al., 2016). In addition, we use daily-averaged UHII to account for both daytime and nighttime urban heat island effects. Although the urban heat island effect is often viewed as a nighttime phenomenon since it often reaches the maximum at night (Oke, 1982; Arnfield, 2003), the nighttime UHII is not used here because previous studies showed that the nighttime UHII was not correlated with the precipitation amount at annual mean scales (Zhao et al., 2014).

All experiments use a global data set, developed by Jackson et al. (2010), for parameterizing urban morphologies (e.g., building height, roof fraction, canyon aspect ratio) and surface materials (e.g., albedo, emissivity, thermal conductivity, heat capacity) of different urban facets. This data set separates the globe into 33 regions and there are 9 regions in our simulation domain (Li et al., 2016b). The data set also includes 4 urban categories including tall building district (TBD), high density (HD), medium density (MD), and low density (LD). However, the current version of LM3-UCM has only one urban category and thus the dominant urban category in each grid cell is considered, which is MD urban for most grid cells. In this study, only grid cells with urban fraction larger than 0.1% are examined. A complete table of input parameters for MD urban can be found in Li et al. (2016b).

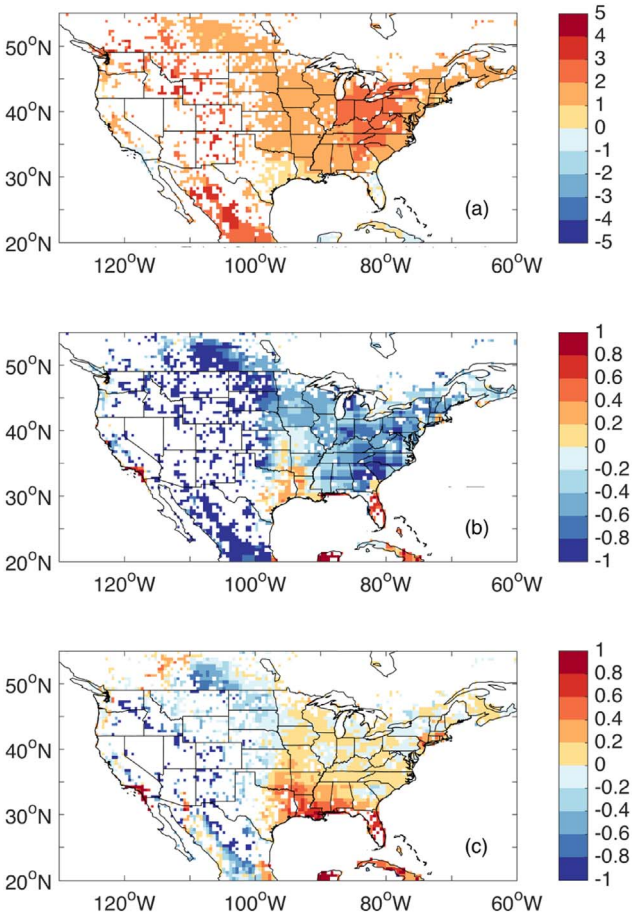

Fig. 2. (a) The summer (June, July, and August) UHIIs (˚C) in Exp. 1 averaged from 1981 to 2000; (b) the difference between Exp. 2 and Exp. 1 (Exp. 2 - Exp. 1, ˚C); (c) The difference between Exp. 3 and Exp. 1 (Exp. 3 - Exp. 1, ˚C).

3. Results

3.1. The relation between UHII and precipitation

Fig. 2a shows the long-term (20-yr) averaged UHII pattern in summer from Exp. 1. The other panels of Fig. 2 show the differences between the other experiments and Exp. 1. It is clear when the Princeton forcing is utilized (Exp. 2, Fig. 2b), the simulated UHIIs are largely reduced across the CONUS. The maximum reduction is 4 K and the average reduction over urban pixels that show reductions is 0.8 K. Exp. 3 with mixed forcing (all forcing variables except precipitation are from ESM2Mb and precipitation is from the Princeton forcing) offers a way to examine the sensitivity of simulated UHII to precipitation. As one can see from Fig. 2c, the simulated UHIIs in Exp. 3, as compared to Exp. 1, show reductions in the west and increases in the east. This pattern is different from that in Fig. 2b. In addition, the magnitudes of these changes in Exp. 3 are on average smaller than their counterparts in Exp. 2. The maximum reduction is still 4 K but the average reduction over urban pixels that show reductions is 0.4 K. The maximum increase is 2.1 K and the average increase over urban pixels that show increases is 0.2 K. The different patterns and magnitudes between Exp. 3 and Exp. 2 clearly suggest the importance of forcing variables other than precipitation. The winter UHIIs have displayed similar features, as shown in Fig. 3. When the Princeton forcing is used to replace the ESM2Mb forcing, the UHIIs are principally reduced (Fig. 3b). When only precipitation is altered (Fig. 3c), the UHIIs are reduced in the west and increased in the east, with smaller magnitudes than those shown in Fig. 3b.

The relation between the precipitation amount and the UHII across the simulated domain (i.e., across cities) is then explored in Fig. 4. In all three experiments, increasing trends of the UHII with increasing precipitation amount are evident in summer (left panels), suggesting that such trends are independent of the atmospheric forcing data sets. The increasing trend of UHII with respect to precipitation across cities over CONUS has been observed in previous studies (Zhao et al., 2014; Li et al., 2016b) and mainly attributed into two factors. Traditionally this is attributed to the increasing evapotranspiration rate of the rural land with precipitation. In wetter climates, the UHII is stronger because the evapotranspiration rate of the rural land is stronger (i.e., the Bowen ratio is smaller) and the rural temperature is lower (Li et al., 2016b; Zhou et al., 2016). This is particularly the case in summer when

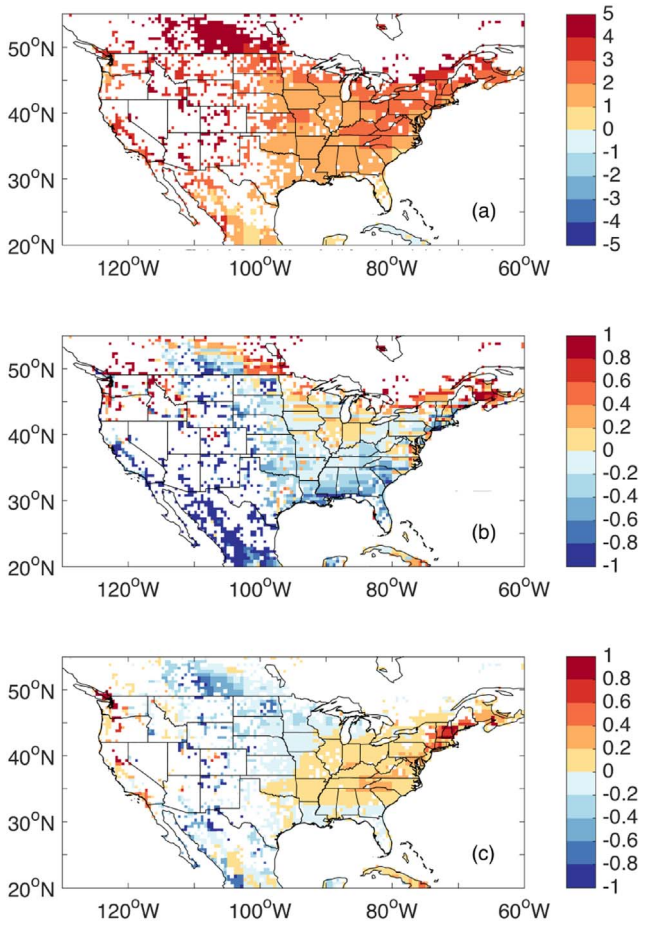

Fig. 3. Same as Fig. 2 but in winter (December, January and February).

the evapotranspiration rate is the largest and more dependent on rainfall (at least over CONUS). A recent study however proposed a different explanation (Zhao et al., 2014). That is, in wetter climates, the rural land has a larger aerodynamic resistance, which leads to a reduced rural near-surface or surface temperature and concomitantly a stronger UHII. The aerodynamic resistance contribution, instead of the Bowen ratio contribution, dominates the correlation between UHII and precipitation across cities (Zhao et al., 2014).

The UHII seems to show a decreasing trend with increasing precipitation amount in winter, especially in Exp. 1 (Fig. 4b). However, such a decreasing trend is mainly caused by the higher UHII when the precipitation amount is smaller than 1 mm/day, beyond which the UHII has nearly no relation with the precipitation amount. In addition, such decreasing trends are not observed in the other two experiments considering the large error bars (Fig. 4d and f). It is interesting to note the dissimilarity between Exp. 1 and the other two, implying that changing precipitation does alter the UHII-precipitation relation in winter. It is equally interesting to note the similarity between Exp. 2 and 3, which suggests that the UHII-precipitation relation is not strongly affected by other atmospheric forcing variables.

There are two possible causes for the dissimilarity between summer and winter from the perspective of evapotranspiration. First, the precipitation includes both liquid and frozen precipitation, which in the model is separated based on whether the air temperature is below the freezing point. In summer, precipitation is dominated by the liquid part, which increases water availability for soil and vegetation to evaporate and transpire, respectively. Because urban areas typically have smaller fractions of soil and vegetation surface, the reduction of urban temperature is not as fast as its rural counterpart as the precipitation amount increases (not shown) and hence the UHII increases with increasing precipitation amount in summer. On the other hand, the frozen precipitation (i.e., snow) increases the albedo of both urban and rural land, and does not cause an obviously dissimilar response of urban and rural temperatures. Therefore, the UHIIs are poorly correlated with the precipitation amount in winter. Second, the UHI effect in summer is sensitive to changes in the evapotranspiration rate, while the UHI effect in winter is also significantly modulated by the building heating, as shown in our previous study (Li et al., 2016b), and the evapotranspiration rate in winter is small in both urban and vegetated rural areas. As a result, the correlations between UHIIs and precipitation amounts are stronger in summer and weaker (or absent) in winter.

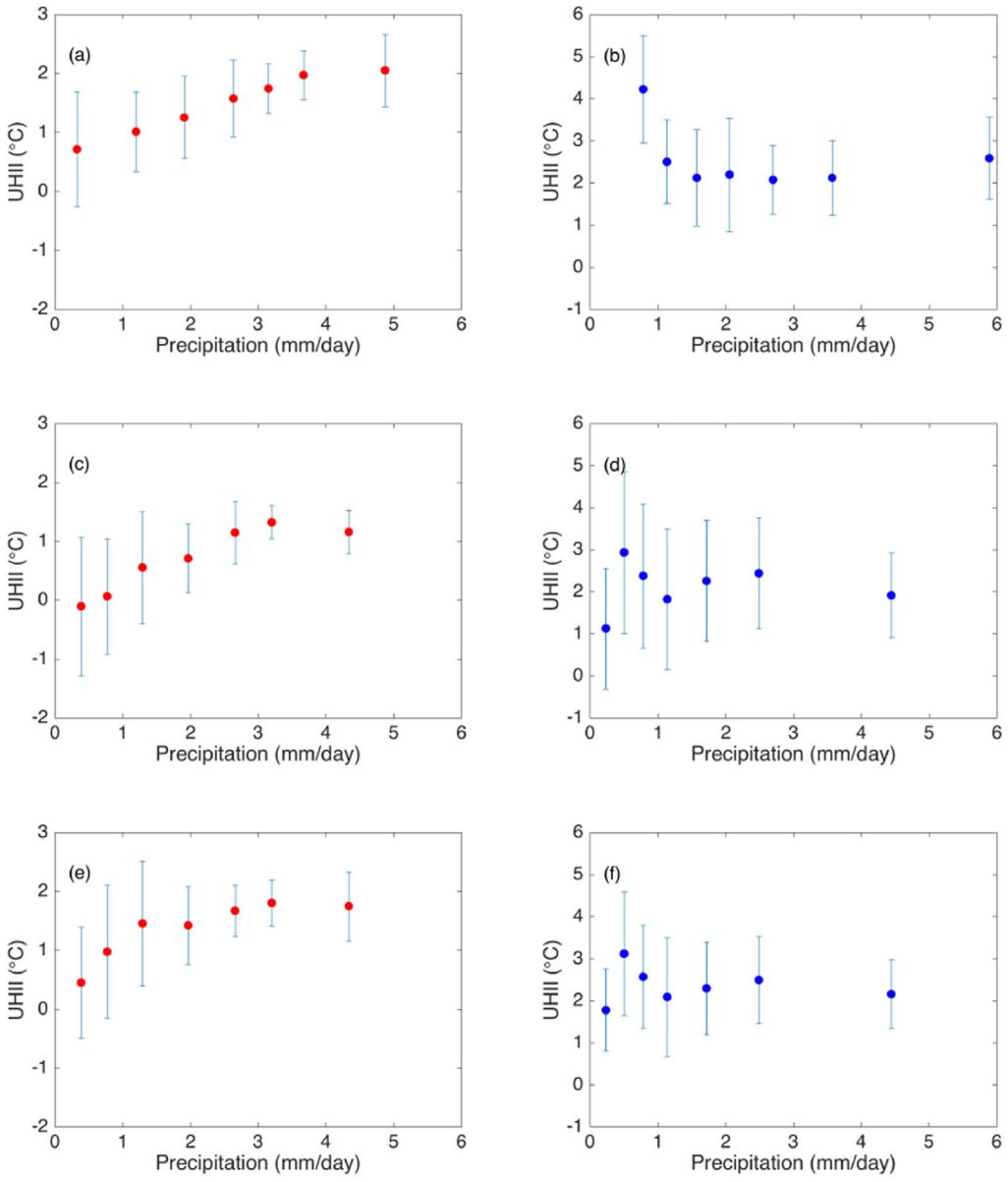

Fig. 4. The relations between precipitation (mm/day) and UHII (°C) (a, c, e) summer, and (b, d, f) winter. (a, b) are results from Exp. 1 using the ESM2Mb forcing; (c, d) are results from Exp. 2 using the Princeton forcing, and (e, f) are results from Exp. 3 using the mixed forcing. The results are bin averaged and the error bars indicate the standard deviation in each bin. Note that each bin has the same number of data points.

3.2. The sensitivity of UHII to precipitation

The model sensitivity of UHII to precipitation ($\partial UHII/\partial P$), defined in Eq. 1, is examined in Fig. 5a (summer) and c (winter). For comparison, we also present R_1 (Fig. 5b and d). Technically any perturbation of P can be used to calculate $\partial UHII/\partial P$. Here we use two data sets that are both reasonable representations of the precipitation climatology to avoid unreasonable and unrealistic ΔP. Note $\Delta UHII$ have been presented in Figs. 2c and 3c for summer and winter, respectively. Comparing Figs. 2c and 3c to Fig. 5 reveals that the pattern of $\partial UHII/\partial P$ is different from that of $\Delta UHII$. This is expected since $\partial UHII/\partial P$ refers to the model sensitivity of UHII to precipitation while $\Delta UHII$ refers to the change of UHII due to changes in precipitation.

In summer (Fig. 5a), the sensitivity of UHII to precipitation is positive over most regions, implying that the UHII increases (decreases) with enhanced (reduced) precipitation. Large values (especially negative values) are observed in the mid-south US (e.g. Mississippi, Arkansas, Missouri, and parts of Texas), suggesting that changes in precipitation will likely result in significant changes in UHIIs in these regions. Sporadic large and positive values are also observed in the western part of the domain. In winter (Fig. 5c), the sensitivity of UHII to precipitation remains sporadic but the magnitude is larger in the northern part of the domain.

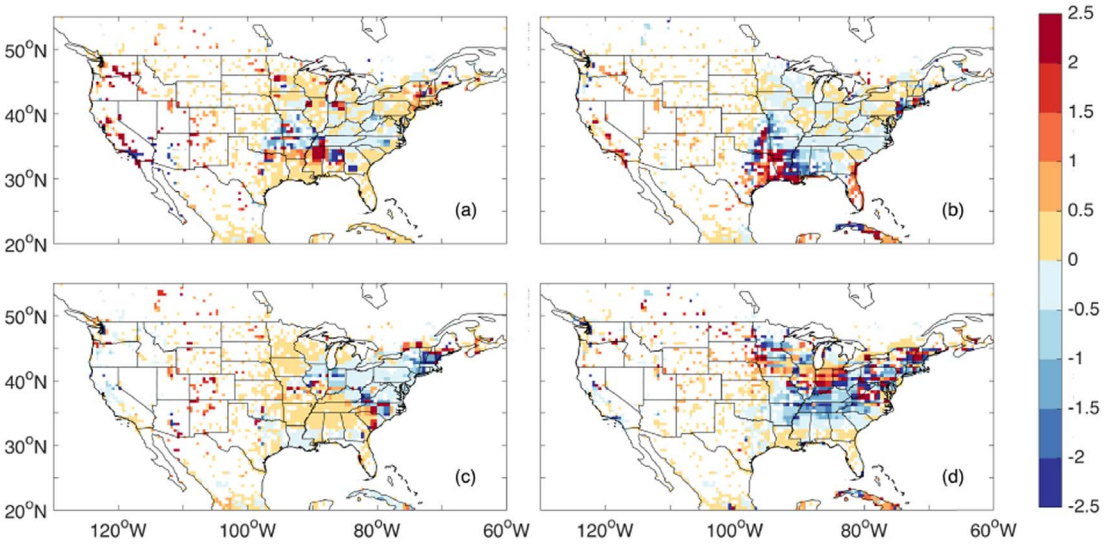

Fig. 5. The summer (a) $\partial UHII/\partial P$ (K day/mm) and (b) R_1 and the winter (c) $\partial UHII/\partial P$ (K day/mm) and (d) R_1.

The results of R_1 show some similarity with those of $\partial UHII/\partial P$ but also important differences (Fig. 5b and d). The similarity comes from the fact that both indicate the effect of precipitation on UHIIs. The differences are expected from their definitions: R_1 is a dimensionless variable calculated as the UHII difference between Exp. 3 and Exp. 1 normalized by the UHII difference between Exp. 2 and Exp. 1; while $\partial UHII/\partial P$ is a dimensional parameter calculated as the UHII difference between Exp. 3 and Exp. 1 normalized by the precipitation difference between Exp. 3 and Exp. 1. The regions where both metrics show large absolute values are broadly consistent (mid and mid-south US in summer and the northeastern part in winter). The absolute values of R_1 averaged over all urban pixels are 1.1 and 1.4 in summer and winter, respectively, suggesting strong contributions of precipitation to UHIIs.

Our results of $\partial UHII/\partial P$ can be compared to a previous study by Zhao et al. (2014), which presented the temporal sensitivity of UHII to precipitation over 65 cities in North America at annual mean scales. In their study, the temporal sensitivity was calculated as the linear regression slope of the annual daytime UHII against the annual precipitation. Offline land simulation results with the Community Land Model showed that the temporal sensitivity was negative in the eastern US and mostly positive in the western US. Remotely sensed land surface temperatures from satellites however showed that negative temporal sensitivities dominate across the domain with only sporadic positive values in the northeastern and northwestern US. They also showed that the temporal sensitivity was negatively correlated with the annual mean precipitation amount in both observations and model simulations.

Fig. 6 shows the sensitivity of UHII to precipitation ($\partial UHII/\partial P$) calculated in our study as a function of precipitation in summer (left) and winter (right). A generally negative trend, which indicates that the UHII under a drier climate is more sensitive to precipitation change, as in Zhao et al. (2014) exists in summer but the scatter is very large. It should be pointed out that the sensitivity defined here is different from that in Zhao et al. (2014): we use the daily average UHI instead of daytime UHI; we use results from all grid cells that have urban fractions larger than zero instead of results from 65 cities; and we use results from two numerical

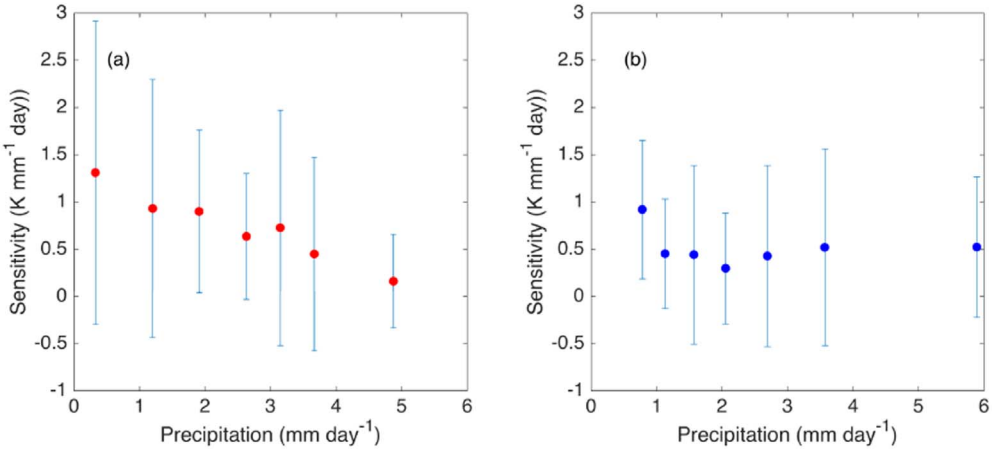

Fig. 6. The sensitivity of UHII to precipitation ($\partial UHII/\partial P$, K day/mm) as a function of precipitation in (a) summer and (b) winter. The precipitation from the ESM2Mb data set is used.

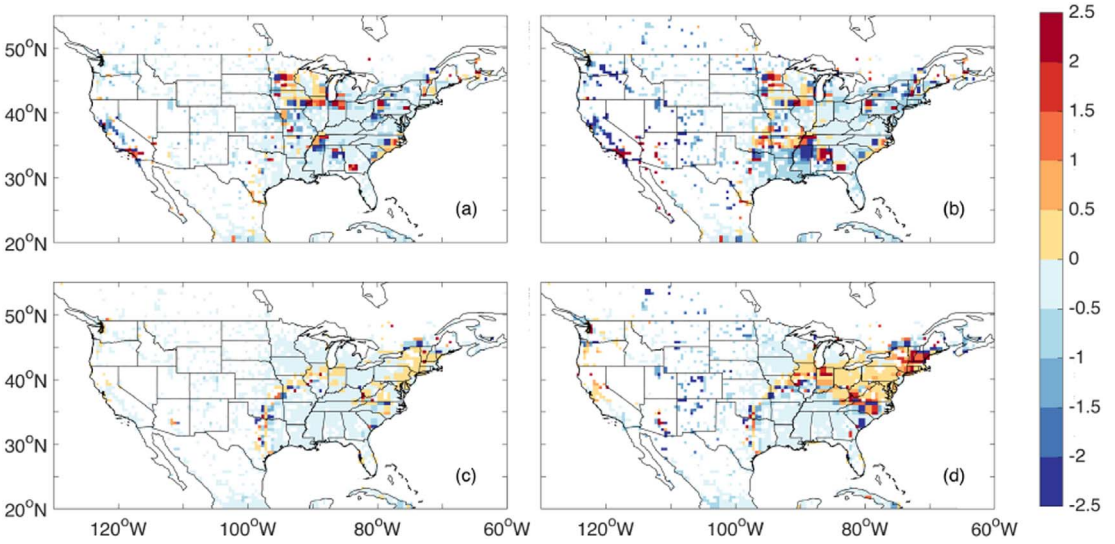

Fig. 7. The summer sensitivities of urban (a) and rural (b) temperatures to precipitation (K day/mm). Their winter counterparts are shown in (c) and (d), respectively.

experiments to calculate the sensitivity instead of applying linear regression to the temporal results.

3.3. Attribution analysis

Before we demystify why certain regions show large sensitivities of UHII to precipitation changes, we examine whether such large sensitivities originate from the urban part or the rural part, as the UHII is defined as the difference between the two. Fig. 7 shows the sensitivities of urban (left panels) and rural (right panels) temperatures to precipitation in summer (top panels) and winter (bottom panels). It becomes evident that the rural temperature actually responds to precipitation change in a more significant way that the urban temperature.

Based on the finding from Fig. 7, Figs. 8 and 9 further explore the sensitivities of key parameters in the surface energy budget (net shortwave radiation, sensible heat flux, latent heat flux, and turbulent transfer coefficient) of the rural land to precipitation in summer and winter, respectively. The sensitivity is again defined as the partial derivative with respect to precipitation (similar to Eq. (1)). It is clear that in summer (Fig. 8), changes in net shortwave radiation (Fig. 8a) are extremely small and do not resemble the pattern of temperature sensitivity (Fig. 7b). Clearly what is more important is the change in the partition between sensible heat flux and latent heat flux, or the Bowen ratio. As one can see, increases (decreases) in the sensible heat flux due to changes in precipitation are nearly balanced by the decreases (increases) in the latent heat flux. Changes in the turbulent transfer coefficient are well correlated with changes in sensible heat flux (Fig. 8b) and temperature (Fig. 7b). In winter (Fig. 9), changes in the Bowen ratio and

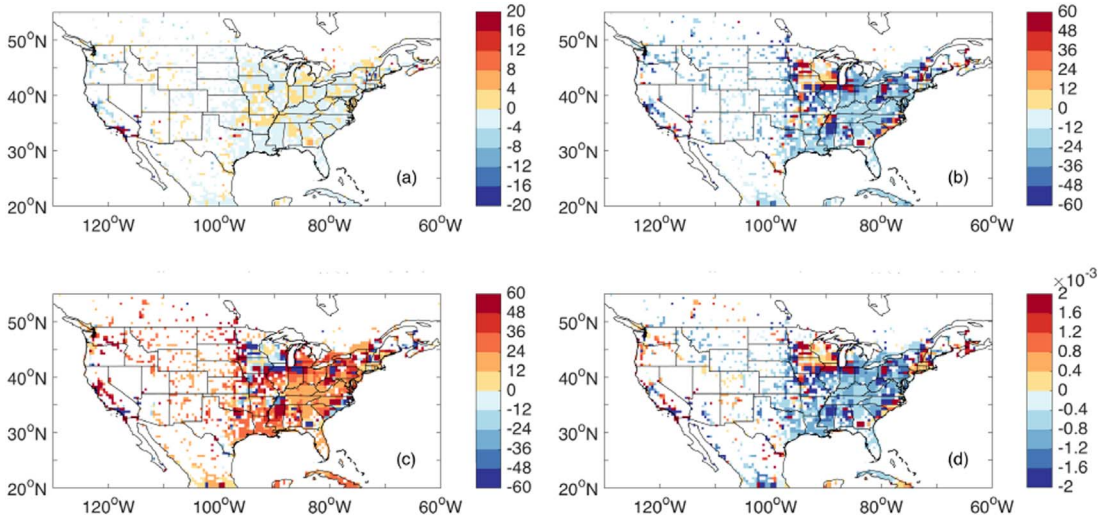

Fig. 8. The sensitivities of (a) net shortwave radiation (W/m^2), (b) sensible heat flux (W/m^2), (c) latent heat flux (W/m^2), and (d) turbulent transfer coefficient of natural vegetation (unitless), to precipitation (mm/day) in summer.

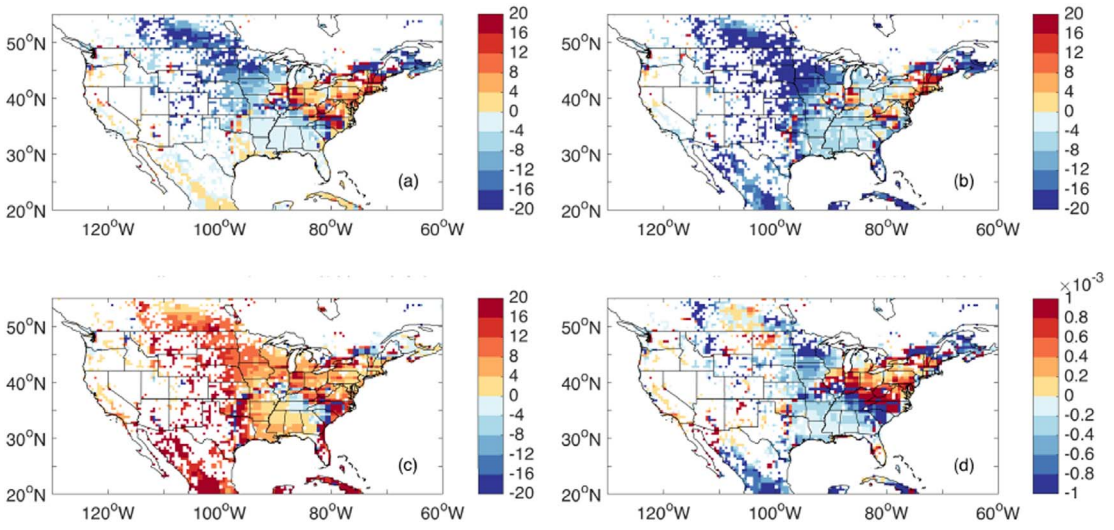

Fig. 9. Same as Fig. 8 except in winter.

turbulent transfer coefficient are also observed as the precipitation changes. However, unlike the minor role played by net shortwave radiation in summer, the sensitivity of net shortwave radiation to precipitation (Fig. 9a) well resembles that of temperature (Fig. 7d), suggesting that changes in the net shortwave radiation also largely contribute to changes in the temperature in winter. This is probably due to the influence of frozen rainfall (i.e., snow), which alters the albedo significantly.

To further estimate the contribution of turbulent transfer coefficient (or the inverse of aerodynamic resistance), the sensible heat flux H (W m^{-2}) is linked to the canopy air temperature T_{ca} (K) through

$$H = \rho c_p C_h U (T_{ca} - T_a), \tag{3}$$

where ρ is the air density (kg m^{-3}), c_p is the specific heat of air under constant pressure (J kg^{-1}), C_h is the turbulent transfer coefficient for heat, U is the wind speed from the atmospheric model (m s^{-1}), T_a is the air temperature from the atmospheric model (K). Note that from Exp. 3 to Exp. 1 the wind speed and air temperature are not altered. As a result, changes in the sensible heat flux between Exp. 3 to Exp. 1 are

$$\Delta H = \rho c_p \Delta C_h U (T_{ca} - T_a) + \rho c_p C_h U \Delta T_{ca}, \tag{4}$$

which is equivalent to

$$\Delta T_{ca} = \frac{\Delta H}{\rho c_p U C_h} - \frac{\Delta C_h H}{\rho c_p U C_h^2} = \Delta T_{ca,H} + \Delta T_{ca,Ch}, \tag{5}$$

where $\Delta T_{ca,H} = \frac{\Delta H}{\rho c_p U C_h}$ and $\Delta T_{ca,Ch} = -\frac{\Delta C_h H}{\rho c_p U C_h^2}$ represent contributions from sensible heat flux change and turbulent transfer coefficient (aerodynamic resistance) change, respectively.

Fig. 10 shows the contributions ($\Delta T_{ca,\ H}$ and $\Delta T_{ca,\ Ch}$) in summer and winter. It is clear that in both summer and winter, the contributions from changes in the turbulent transfer coefficient are much smaller compared to the counterparts due to sensible heat flux changes, suggesting a less important role of aerodynamic resistance in controlling the sensitivity of rural temperature to precipitation. This further anchors the important role of Bowen ratio in summer and winter, as well as the snow albedo effect in winter, in controlling the sensitivity of UHII to precipitation through controlling the sensible heat flux.

Our attribution results are different from a previous study (Zhao et al., 2014), which used an intrinsic biophysical mechanism method to attribute the surface UHII to contributions from albedo, aerodynamic resistance, the Bowen ratio, ground heat flux, and anthropogenic heat flux. They showed that the aerodynamic resistance contribution dominates the spatial correlation between UHII and precipitation at annual mean scales. In our study, the aerodynamic resistance seems to play a minor role in modulating the sensitivity of rural temperature to precipitation. Such differences can be caused by the different urban and land model structures and the different attribution methods used in their study and our work. This calls for an intercomparison among models in terms of the simulated urban climate and more investigations into the attribution of UHII over a large domain with different climates.

4. Conclusions

This paper aims to examine the sensitivity of urban heat islands to precipitation changes at climate scales. We calculate the sensitivity of urban heat island intensity (UHII) to precipitation using two numerical experiments in which only the precipitation forcing is altered. We also compare the contribution of precipitation to those of other atmospheric forcing variables. Results show that only altering the precipitation forcing from the ESM2Mb to the Princeton data sets leads to negative changes in UHIIs in the west and

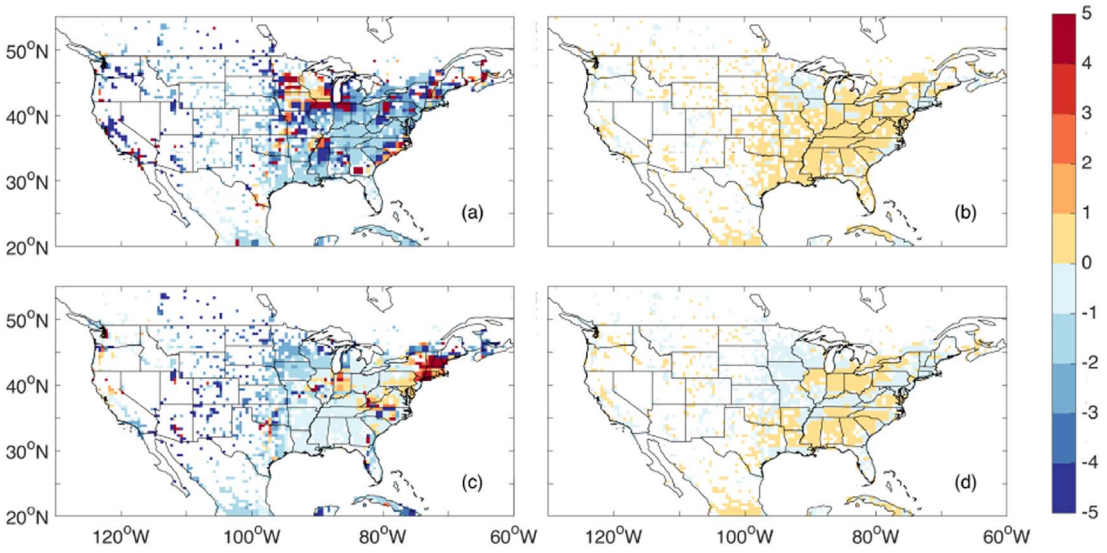

Fig. 10. $\Delta T_{ca,H}$ (a, c) and $\Delta T_{ca,Ch}$ (b, d) of natural vegetation normalized by ΔP in summer (a, b) and winter (c, d). The unit is K day/mm.

northwest, and positive changes in UHIIs in the southeast of CONUS. The sign of such changes is determined by two factors, changes in precipitation (ΔP) and the sensitivity of UHII to precipitation ($\partial UHII/\partial P$). Changes in precipitation (ΔP) are imposed and can be different for different senarios (e.g., if we were to study future changes in the UHII due to changes in precipitation, ΔP will be different from the values used here). As such, what is more important is the sensitivity of UHII to precipitation.

Our model results indicate that the summer sensitivity of UHII to precipitation ($\partial UHII/\partial P$) is largely positive except in the mid-south US. The winter sensitivity of UHII to precipitation is negative in northeastern US, implying that the UHII will be enhanced under drier conditions. Our results suggest that the relation between UHII and precipitation has a strong seasonality, and the positive correlation between the UHII and the precipitation amount at annual mean scales observed in previous studies comes from the summer season. Our results further suggest that the observed negative correlation between the sensitivity of UHII and the precipitation amount at annual mean scales also mainly comes from the summer season.

Close inspection reveals that the large sensitivities of UHII to precipitation are mainly caused by the response of rural temperatures, rather than urban temperatures, to precipitation changes. The rural temperatures are sensitive to precipitation change due to the Bowen ratio effect in summer and the Bowen ratio and the snow albedo effects in winter. Unlike previous studies suggesting an important role of aerodynamic resistance (Zhao et al., 2014), the contribution from change in the turbulent transfer coefficient or aerodynamic resistance, as compared to the contribution from change in the sensible heat flux, is found to be small in our study.

Another way to quantify the contribution of precipitation is to compare changes in the UHII induced by changes in precipitation to those induced by changes in all atmospheric forcing variables, namely, R_1 in Eq. (2). Different from $\partial UHII/\partial P$, R_1indicates the importance of precipitation relative to the other atmospheric forcing variables. It is interesting to observe that the patterns of $\partial UHII/\partial P$ and R_1 have similarity. Regions with large absolute $\partial UHII/\partial P$ values generally coincide with those with large absolute R_1 values, which again include the mid-south in summer and the northeast in winter. The mean absolute values of R_1 are larger than 1 in both summer and winter, suggesting strong contributions of precipitation to UHIIs.

In summary, the answers to the questions raised in the introduction are:

1) Yes, the atmospheric forcing is very important. In our study, altering precipitation alone by replacing the ESM2Mb forcing with the Princeton data can change the simulated summertime UHII by as much as 4 K over the CONUS.
2) Yes, there are places where the UHII is very sensitive to precipitation changes. These regions are primarily located in the mid-south of US for the summer season and the northeastern US for the winter season. These hot spots are mainly caused by the response of rural temperatures, rather than urban temperatures, to precipitation changes.

At the end, it is important to point out the limitations of our study. First, while the LM3-UCM parameterizes key processes associated with both liquid and frozen precipitation in urban environments (Li et al., 2016a), the current experimental design does not consider river routine and thus the influence of precipitation on near-surface temperature is limited to be within the same grid cell. The metrics (including the sensitivity and R_1) are also derived based on local UHII and local precipitation. We note that such a local approach has been also used in previous studies (Zhao et al., 2014) and incorporating non-local effects is left for future investigations. Second, our metrics are derived based on monthly averaged UHII and precipitation data instead of instantaneous values. The non-linearity in the metrics may introduce some biases in our results but we expect these biases to be small given our focus on the long-term climate scales as well as the use of offline land simulations. Third, while our method of studying the sensitivity of land surface states (in this case urban and rural temperatures) to atmospheric forcing through utilizing different forcing data sets is

not uncommon (Sheffield et al., 2006; Reichle et al., 2011), it is still possible that mixing different forcing data sets might create some inconsistency, especially when model outputs and observational data are combined. Another possible method to explore in future work is to alter the precipitation forcing by a certain amount (either a fixed amount or a relative proportion). Last but not least, our study only examines the sensitivity of simulated UHII to precipitation, which might be model dependent (including the urban model and the land model that simulates the vegetation tiles), as suggested by the difference between our work and previous studies. Intercomparison among models is strongly needed, which can be facilitated by The Land Use Model Intercomparison Project (LUMIP) within Coupled Model Intercomparison Project Phase 6 (CMIP6) (Lawrence et al., 2016).

Acknowledgements

This research is funded by the Undergraduate Research Opportunities Program (UROP) of Boston University. The simulations were conducted at GFDL. We thank Dr. Sergey Malyshev and Dr. Elena Shevliakova at GFDL for their help with performing and analyzing the simulations. We also thank the two reviewers whose comments led to significant improvements of the manuscript.

References

Akbari, H., Pomerantz, M., Taha, H., 2001. Cool surfaces and shade trees to reduce energy use and improve air quality in urban areas. Sol. Energy 70, 295–310.
Anderson, B.G., Bell, M.L., 2009. Weather-related mortality: how heat, cold, and heat waves affect mortality in the United States. Epidemiology 20, 205–213.
Arnfield, A.J., 2003. Two decades of urban climate research: a review of turbulence, exchanges of energy and water, and the urban heat island. Int. J. Climatol. 23, 1–26.
Best, M.J., Grimmond, C.S.B., 2015. Key conclusions of the first international urban land surface model comparison project. Bull. Am. Meteorol. Soc. 96 (805-U18).
Dunne, J.P., John, J.G., Adcroft, A.J., Griffies, S.M., Hallberg, R.W., Shevliakova, E., Stouffer, R.J., Cooke, W., Dunne, K.A., Harrison, M.J., Krasting, J.P., Malyshev, S.L., Milly, P.C.D., Phillipps, P.J., Sentman, L.T., Samuels, B.L., Spelman, M.J., Winton, M., Wittenberg, A.T., Zadeh, N., 2012. GFDL's ESM2 global coupled climate–carbon earth system models. Part I: physical formulation and baseline simulation characteristics. J. Clim. 25, 6646–6665.
Dunne, J.P., John, J.G., Shevliakova, E., Stouffer, R.J., Krasting, J.P., Malyshev, S.L., Milly, P.C.D., Sentman, L.T., Adcroft, A.J., Cooke, W., Dunne, K.A., Griffies, S.M., Hallberg, R.W., Harrison, M.J., Levy, H., Wittenberg, A.T., Phillips, P.J., Zadeh, N., 2013. GFDL's ESM2 global coupled climate-carbon earth system models. Part II: carbon system formulation and baseline simulation characteristics. J. Clim. 26, 2247–2267.
Fan, Y.F., Li, Y.G., Wang, X.X., Catalano, F., 2016. A new convective velocity scale for studying diurnal urban heat island circulation. J. Appl. Meteorol. Clim. 55, 2151–2164.
Fernando, H.J.S., Zajic, D., Di Sabatino, S., Dimitrova, R., Hedquist, B., Dallman, A., 2010. Flow, turbulence, and pollutant dispersion in urban atmospheres. Phys. Fluids 22.
Grimm, N.B., Faeth, S.H., Golubiewski, N.E., Redman, C.L., Wu, J.G., Bai, X.M., Briggs, J.M., 2008. Global change and the ecology of cities. Science 319, 756–760.
Grimmond, C.S.B., 2007. Urbanization and global environmental change: local effects of urban warming. Geogr. J. 173, 83–88.
Grimmond, C.S.B., Blackett, M., Best, M.J., Baik, J.J., Belcher, S.E., Beringer, J., Bohnenstengel, S.I., Calmet, I., Chen, F., Coutts, A., Dandou, A., Fortuniak, K., Gouvea, M.L., Hamdi, R., Hendry, M., Kanda, M., Kawai, T., Kawamoto, Y., Kondo, H., Krayenhoff, E.S., Lee, S.H., Loridan, T., Martilli, A., Masson, V., Miao, S., Oleson, K., Ooka, R., Pigeon, G., Porson, A., Ryu, Y.H., Salamanca, F., Steeneveld, G.J., Tombrou, M., Voogt, J.A., Young, D.T., Zhang, N., 2011. Initial results from phase 2 of the international urban energy balance model comparison. Int. J. Climatol. 31, 244–272.
Grimmond, C.S.B., Blackett, M., Best, M.J., Barlow, J., Baik, J.J., Belcher, S.E., Bohnenstengel, S.I., Calmet, I., Chen, F., Dandou, A., Fortuniak, K., Gouvea, M.L., Hamdi, R., Hendry, M., Kawai, T., Kawamoto, Y., Kondo, H., Krayenhoff, E.S., Lee, S.H., Loridan, T., Martilli, A., Masson, V., Miao, S., Oleson, K., Pigeon, G., Porson, A., Ryu, Y.H., Salamanca, F., Shashua-Bar, L., Steeneveld, G.J., Tombrou, M., Voogt, J., Young, D., Zhang, N., 2010. The international urban energy balance models comparison project: first results from phase 1. J. Appl. Meteorol. Clim. 49, 1268–1292.
Hidalgo, J., Masson, V., Gimeno, L., 2010. Scaling the daytime urban heat island and urban-breeze circulation. J. Appl. Meteorol. Clim. 49, 889–901.
Hoffmann, P., Krueger, O., Schlunzen, K.H., 2012. A statistical model for the urban heat island and its application to a climate change scenario. Int. J. Climatol. 32, 1238–1248.
Jackson, T.L., Feddema, J.J., Oleson, K.W., Bonan, G.B., Bauerc, J.T., 2010. Parameterization of urban characteristics for global climate modeling. Ann. Assoc. Am. Geogr. 100, 848–865.
Lawrence, D.M., Hurtt, G.C., Arneth, A., Brovkin, V., Calvin, K.V., Jones, A.D., Jones, C.D., Lawrence, P.J., de Noblet-Ducoudre, N., Pongratz, J., Seneviratne, S.I., Shevliakova, E., 2016. The land use model intercomparison project (LUMIP) contribution to CMIP6: rationale and experimental design. Geosci. Model Dev. 9, 2973–2998.
Li, D., Bou-Zeid, E., 2013. Synergistic interactions between urban heat islands and heat waves: the impact in cities is larger than the sum of its parts. J. Appl. Meteorol. Clim. 52, 2051–2064.
Li, D., Malyshev, S., Shevliakova, E., 2016a. Exploring historical and future urban climate in the earth system modeling framework: 1. Model development and evaluation. J. Adv. Model Earth Syst. 8, 917–935.
Li, D., Malyshev, S., Shevliakova, E., 2016b. Exploring historical and future urban climate in the earth system modeling framework: 2. Impact of urban land use over the Continental United States. J. Adv. Model Earth Syst. 8, 936–953.
Li, D., Sun, T., Liu, M., Wang, L., Gao, Z., 2016. Changes in wind speed under heat waves enhance urban heat islands in the Beijing metropolitan area. J. Appl. Meteorol. Clim. 55, 2369–2375.
Loridan, T., Grimmond, C.S.B., Grossman-Clarke, S., Chen, F., Tewari, M., Manning, K., Martilli, A., Kusaka, H., Best, M., 2010. Trade-offs and responsiveness of the single-layer urban canopy parametrization in WRF: An offline evaluation using the MOSCEM optimization algorithm and field observations. Q. J. R. Meteorol. Soc. 136, 997–1019.
Malyshev, S., Shevliakova, E., Stouffer, R.J., Pacala, S.W., 2015. Contrasting local vs. regional effects of land-use-change induced heterogeneity on historical climate: analysis with the GFDL earth system model. J. Clim. 28, 5448–5469.
Mills, G., 2008. Luke Howard and the climate of London. Weather 63, 153–157.
Milly, P.C.D., Malyshev, S.L., Shevliakova, E., Dunne, K.A., Findell, K.L., Gleeson, T., Liang, Z., Phillipps, P., Stouffer, R.J., Swenson, S., 2014. An enhanced model of land water and energy for global hydrologic and earth-system studies. J. Hydrometeorol. 15, 1739–1761.
Oke, T.R., 1973. City size and the urban heat island. Atmos. Environ. 7, 769–779 (1967).
Oke, T.R., 1981. Canyon geometry and the nocturnal urban heat-island - comparison of scale model and field observations. J. Climatol. 1 (237-&).
Oke, T.R., 1982. The energetic basis of the urban heat-island. Q. J. R. Meteorol. Soc. 108, 1–24.
Reichle, R.H., Koster, R.D., De Lannoy, G.J.M., Forman, B.A., Liu, Q., Mahanama, S.P.P., Toure, A., 2011. Assessment and enhancement of MERRA land surface hydrology estimates. J. Clim. 24, 6322–6338.
Rizwan, A.M., Dennis, Y.C.L., Liu, C.H., 2008. A review on the generation, determination and mitigation of urban heat island. J. Environ. Sci. China 20, 120–128.
Rosenzweig, C., Solecki, W., Hammer, S.A., Mehrotra, S., 2010. Cities lead the way in climate-change action. Nature 467, 909–911.
Ryu, Y.H., Baik, J.J., Lee, S.H., 2011. A new single-layer urban canopy model for use in mesoscale atmospheric models. J. Appl. Meteorol. Clim. 50, 1773–1794.
Sarrat, C., Lemonsu, A., Masson, V., Guedalia, D., 2006. Impact of urban heat island on regional atmospheric pollution. Atmos. Environ. 40, 1743–1758.

Schatz, J., Kucharik, C.J., 2014. Seasonality of the urban heat island effect in Madison, Wisconsin. J. Appl. Meteorol. Clim. 53, 2371–2386.
Sheffield, J., Goteti, G., Wood, E.F., 2006. Development of a 50-year high-resolution global dataset of meteorological forcings for land surface modeling. J. Clim. 19, 3088–3111.
Shevliakova, E., Pacala, S.W., Malyshev, S., Hurtt, G.C., Milly, P.C.D., Caspersen, J.P., Sentman, L.T., Fisk, J.P., Wirth, C., Crevoisier, C., 2009. Carbon cycling under 300 years of land use change: importance of the secondary vegetation sink. Glob. Biogeochem. Cyles 23.
Stone, B., 2012. The city and the coming climate: climate change in the places we live. Cambridge University Press, New York.
Theeuwes, N.E., Steeneveld, G.J., Ronda, R.J., Holtslag, A.A.M., 2017. A diagnostic equation for the daily maximum urban heat island effect for cities in northwestern Europe. Int. J. Climatol. 37, 443–454.
United Nations D o E a S A, Population Division, 2014. World Urbanization Prospects: The 2014 Revision, Highlights. United Nations, New York.
Wang, Z.H., Bou-Zeid, E., Au, S.K., Smith, J.A., 2011. Analyzing the sensitivity of WRF's single-layer urban canopy model to parameter uncertainty using advanced Monte Carlo simulation. J. Appl. Meteorol. Clim. 50, 1795–1814.
Wiesner, S., Eschenbach, A., Ament, F., 2014. Urban air temperature anomalies and their relation to soil moisture observed in the city of Hamburg. Meteorol. Z. 23, 143–157.
Zhao, L., Lee, X., Smith, R.B., Oleson, K., 2014. Strong contributions of local background climate to urban heat islands. Nature 511, 216–219.
Zhou, D., Li, D., Sun, G., Zhang, L., Liu, Y., Hao, L., 2016. Contrasting effects of urbanization and agriculture on surface temperature in eastern China. J. Geophys. Res. Atmos. 121, 9597–9606.
Zhou, D.C., Zhang, L.X., Li, D., Huang, D.A., Zhu, C., 2016. Climate-vegetation control on the diurnal and seasonal variations of surface urban heat islands in China. Environ. Res. Lett. 11.